JOURNAL OF SPACECRAFT AND ROCKETS
Vol. 34, No. 1, January–February 1997

Planning Spiral Motions of Nonholonomic Free-Flying Space Robots

Y. Nakamura* and T. Suzuki*
University of Tokyo, Tokyo 113, Japan

The orientation of a space satellite may change due to the actuation of an attached manipulator. Such a motion is subject to the nonintegrable and, therefore, nonholonomic constraints induced by the angular momentum conservation. Some of the previous literature proposed methods to produce a desired change of the satellite orientation by controlling the attached manipulator. These methods treated the point-to-point control problem mainly and, thus, one cannot apply them to the path-tracking problem. The path-tracking problem of an arbitrary trajectory of nine dimensions, which consists of six dimensions for the manipulator joints and three dimensions for the satellite orientation, is discussed. The main scenario is that because such a trajectory is generally infeasible, we search for a feasible motion that approximates the desired trajectory within a designated margin. We name the motion the "spiral motion." A computational scheme for planning the spiral motion is presented, and this is followed by computer simulation that illustrates the effectiveness of the scheme. The relationship of singular points with computational convergency is also discussed.

Nomenclature

$\boldsymbol{a}, \boldsymbol{b}, \boldsymbol{c}$	= parameters of the closed-path motion
$\|\boldsymbol{a}\|_W$	= $\boldsymbol{W}$-weighted norm of $\boldsymbol{a}$, $\sqrt{(\boldsymbol{a}^T \boldsymbol{W}\boldsymbol{a})}$
C	= closed path in the end-effector coordinates space
$\boldsymbol{D}$	= the effect of the closed-path motion
$\boldsymbol{D}_{ij}$	= (i, j) element of $\boldsymbol{D}$ defined by Eq. (15), $\in \boldsymbol{S}^3$
D_{ijk}	= kth element of $\boldsymbol{D}_{ij}$ ($k = 0, \ldots, 3$)
$d()$	= differential form (Refs. 9 and 10) of ( )
$d\boldsymbol{x}$	= 1-form (Ref. 9)
$d(d\boldsymbol{x})$	= 2-form (Ref. 9)
E	= area enclosed by s_1 and s_2 or its value such that $dE \overset{\text{def}}{=} ds_1 \wedge ds_2$
$\boldsymbol{f}_i$	= vector defined by Eq. (B3)
$\boldsymbol{H}$	= 4×6 Jacobian from the joint coordinates to the satellite orientation in Eq. (1), $\partial\boldsymbol{\epsilon}/\partial\boldsymbol{q}$
$\boldsymbol{I}$	= identity matrix
$\boldsymbol{J}$	= 7×6 generalized Jacobian (Refs. 1 and 8) from the joint coordinates to the end-effector coordinates in Eq. (2), $\partial\boldsymbol{u}/\partial\boldsymbol{q}$
J	= augmented criterion, Eq. (B5)
L	= weight for length in $\boldsymbol{W}$, m
n	= spiral pitch
Q	= criterion
$\boldsymbol{q}$	= joint coordinates, $\in \boldsymbol{R}^6$
q_i	= ith component of $\boldsymbol{q}$, or the angle of ith joint, rad
S	= area enclosed by C
s_1, s_2	= time-periodic functions with the period Δt
$\boldsymbol{u}$	= end-effector coordinates (position and orientation), $\in \boldsymbol{R}^3 \times \boldsymbol{S}^3$
$\boldsymbol{v}_e$	= linear velocity of the end effector in Eq. (16)
$\boldsymbol{W}$	= nondimensionalizing matrix, diag $(1/L^2, 1/L^2, 1/L^2, 1, 1, 1, 1)$
$\boldsymbol{X}$	= 11×7 Jacobian from the joint coordinates to the generalized coordinates, $(\boldsymbol{Y}^T, \boldsymbol{I}^T)^T$
$\boldsymbol{X}_i$	= ith column vector of $\boldsymbol{X}$, $\in \boldsymbol{S}^3 \times \boldsymbol{R}^3 \times \boldsymbol{S}^3$
$\boldsymbol{X}_n$	= matrix $\boldsymbol{X}$ when actuated by the nominal end-effector motion $\boldsymbol{u}_n$
$\boldsymbol{x}$	= generalized coordinates of the space robot, $(\boldsymbol{\epsilon}^T, \boldsymbol{u}^T)^T$
$\boldsymbol{Y}$	= 4×7 Jacobian from the end-effector coordinates to the satellite orientation, $\boldsymbol{H}\boldsymbol{J}^\sharp$
$\boldsymbol{Y}_i$	= ith column vector of $\boldsymbol{Y}$, $\in \boldsymbol{S}^3$
$\Delta()$	= change of ( ) in Δt
Δt	= spiral period, s
$\Delta\boldsymbol{\epsilon}_{cd}$	= desired change of the satellite orientation for the closed path, $\Delta\boldsymbol{\epsilon}_d - \Delta\boldsymbol{\epsilon}_n$
$\boldsymbol{\epsilon}$	= satellite orientation [represented by Euler parameters (Refs. 11 and 12)]
$\boldsymbol{\lambda}$	= Lagrange multiplier
$\boldsymbol{\xi}$	= Gibbs vector
σ	= spiral radius, $\|\boldsymbol{a}\|_W$
σ_d	= upper limit of the spiral radius
ϕ	= spiral frequency, or the angular frequency of the closed-path motion, $2\pi/\Delta t$, rad/s
ϕ_n	= spiral frequency for n pitches
ϕ_1	= spiral frequency for a single-turn spiral motion
$\boldsymbol{\omega}$	= angular velocity of the satellite, $\in \boldsymbol{R}^3$
$\boldsymbol{\omega}_e$	= angular velocity of the end effector in Eq. (16)
$\wedge$	= exterior derivative (Ref. 9)

Subscripts

c	= closed-path motion element
d	= desired value
n	= nominal motion element
p	= positional element
q	= for expression by joint coordinates
ϵ	= orientational element
0	= initial value

Superscripts

(i)	= ith iterated value
$\sharp$	= pseudoinverse matrix

I. Introduction

A FREE-FLYING space robot is subject to the momentum and angular momentum conservation laws. It is well known that the angular momentum conservation law is nonintegrable and, therefore, nonholonomic.[1] Since the momentum conservation law forms a set of holonomic constraints, the generalized coordinates of a free-flying space robot consist of the those for the satellite orientation and those for the manipulator configurations. Therefore, a free-flying space robot with a six-degree-of-freedom (DOF) manipulator, for example, has nine generalized coordinates. Generally, it is impossible to follow an arbitrarily given nine-dimensional trajectory of the generalized coordinates with only the manipulator joints' motion, if an orientation control device such as a control moment

Received Dec. 3, 1995; revision received Aug. 2, 1996; accepted for publication Aug. 15, 1996. Copyright © 1996 by the American Institute of Aeronautics and Astronautics, Inc. All rights reserved.

*Department of Mechano-Informatics, 7-3-1 Hongo, Bunkyo-ku.

gyro is not equipped on the satellite. However, it was shown that a free-flying space robot without an orientation control device is locally controllable.[1] This implies that though it is impossible to follow an arbitrary given trajectory, it is possible to reach an arbitrary point in the generalized coordinates starting from an arbitrary initial point only if the nonholonomic constraints are carefully considered in planning and control. Although we assume it from pure technical point of view, there are various possible advantages for the system without any special orientation control device. 1) One may consider the case of malfunction or breakdown of the device. 2) One may wish to minimize the use of the device, if it consists of thrusters that use limited and expensive fuel. 3) Even when the device consists of wheels, one may find frequent or continuous actuation of wheels takes too much electricity. 4) The future designer of small space robot services may choose not to have such a heavy and bulky device if a robot can live without it.

The motion control of free-flying space robots has two major problems as a consequence of nonholonomic constraints: 1) Path planning and 2) feedback control have been already studied in depth for the conventional fixed-base manipulators. They are, however, not as intuitive for the free-flying space robots as those for the fixed-base manipulators.

The path planning of the fixed-base manipulators needs to consider only the environmental constraints that are commonly holonomic and, therefore, geometric, whereas that of the free-flying space robot requires one to take account of the nonholonomic, namely, differential-geometric constraints in addition to the environmental ones. This is what leads to the fact that many of intuitive path planning algorithms developed for robots with holonomic constraints become inapplicable. Vafa and Dubowsky[2] proposed a method to minimize the disturbance of satellite orientation by cyclic motions of a manipulator. Nakamura and Mukherjee[1] proposed a method of finding a solution by using a Lyapunov function and called it a bidirectional approach. Senda et al.[3] obtained a trajectory using a neural network. Akiyama and Sakawa[4] obtained an optimal trajectory for planar 2-link robots and three-dimensional 3-link robots using nonlinear programming method. Yamada[5] used the variational method to find a closed trajectory of manipulator joints that generates an arbitrary change of satellite attitude.

The feedback control of free-flying space robots is difficult in particular because they fall in the class of a nonlinear system that is not stabilizable with smooth and static feedback control law.[6] Only a few works have been published on this issue. Sampei et al.[7] proposed feedback stabilization of a simple free-flying space robot.

We propose a method to approximate an arbitrary nine-dimensional trajectory that is planned rather intuitively without taking into account the nonholonomic constraints, by introducing a spiral-like perturbation around the nine-dimensional trajectory. The perturbation is determined by carefully considering the nonholonomic constraints. One of the advantages of this approach is that the already developed path-planning algorithms for the conventional robots can be tied to a nonholonomic path-planning algorithm. This what divides the large path-planning problem into two subproblems, one which considers only the environmental constraints and the other takes care of the nonholonomic ones. The spiral-like perturbation is designed around the six-dimensional components that correspond to the end-effector motion, such that it causes an appropriate change of the remaining three components. It is a theoretical feature that the method approximates an arbitrary trajectory in the nine-dimensional generalized coordinates with an arbitrary small nonzero error. The method can be extended to free-flying space robots with a manipulator of higher DOF and with multiple manipulators, in a straightforward manner. Another advantage is that the spiral motion restores the configuration of the system as desired at each end of the period and limits the deviation from the desired configuration within an arbitrary designated margin.

II. Spiral Motion

A. Concept

First, we explain the concept of spiral motion rather intuitively, before describing the detailed discussion. We consider a satellite and a six-DOF manipulator on it. Although there could be more the DOF of the manipulator, we would limit the focus to this minimum but common situation. When the attitude control device of the satellite is not used, the whole system is represented by nine generalized coordinates, (six of the manipulator joints and three of the satellite orientation) being driven by six joint actuators.

The six generalized coordinates of the manipulator may be represented by the position and orientation of the end effector except for the singular cases. When an arbitrary trajectory is given for the nine generalized coordinates to trace, it is generally infeasible with six joint actuators. Umetani and Yoshida[8] proposed to follow the end-effector trajectory disregarding the satellite orientation. The satellite will have $\Delta\epsilon_n$ as a side effect that depends on the nominal end-effector motion $\boldsymbol{u}_n(t)$. Yamada[5] computed an optimal closed path of the joint space that yields the designated change of the satellite orientation and minimizes the radius of the closed path. It will also be possible to find a closed path $\boldsymbol{u}_c(t)$ of the end effector that changes the satellite orientation into the designated configuration.

A simple addition of the paths $\boldsymbol{u}_n + \boldsymbol{u}_c$ traces a single-turn spiral-like path. The radius of $\boldsymbol{u}_c$ is referred to as the spiral radius of $\boldsymbol{u}_n + \boldsymbol{u}_c$. The corresponding satellite orientation change becomes nearly $\Delta\epsilon_n + \Delta\epsilon_c$, although this simple addition is not exact due to nonlinearity. If we divide $\boldsymbol{u}_n$ into small parts and find a closed path of the end effector for each of them, the spiral becomes multiturn and the spiral radii get smaller, which is explained in Sec. III.D. In this way, we would be able to find the closed paths such that the trajectory of the satellite orientation approximately follows an arbitrary given one. The resultant motion of the whole system caused by the multiturn spiral end-effector motion is considered an approximation of an arbitrarily given nine-dimensional trajectory of the end-effector coordinates $\boldsymbol{u}_n$ and the satellite orientation ϵ_d that is physically infeasible in general. The smaller the division of the end-effector path becomes, the more the spiral radii reduce and the better the approximation becomes. From this point of view, it would be possible to approximate a given nine-dimensional trajectory with arbitrary specified nonzero error. If the given desired trajectory includes temporal requirements, the approximation with smaller radii results in larger velocity along the path since the length of path to trace in the given time becomes larger. In the sections that follow, we formulate this problem mathematically and develop the computational scheme of the minimal spiral motion, where the exact nonlinearity is to be taken into consideration.

B. Generalized Coordinates

Yamada[5] takes the manipulator joint coordinates $\boldsymbol{q}$ and the satellite orientation ϵ as generalized coordinates and computes a closed path of $\boldsymbol{q}$ that generates the desired change of ϵ after a cycle. This problem was solved as an optimization in the Euclidean space $\boldsymbol{R}^6$ of the joints. Because the trajectory control of an end effector is important in practice, we consider $\boldsymbol{u}$ as parts of the generalized coordinates instead of joint coordinates. The two choices of generalized coordinates are physically equivalent except for the singularity cases.

We use the Euler parameters as an expression of orientation. We briefly summarize the definition and properties of the Euler parameters in the first subsection of Appendix A. Since we take $\boldsymbol{u}$ as generalized coordinates instead of $\boldsymbol{q}$, our trajectory planning problem lies not in an Euclidean space $\boldsymbol{R}^6$ but in a non-Euclidean space $\boldsymbol{R}^3 \times \boldsymbol{S}^3$.

The satellite orientation velocity is expressed in terms of the joint angle velocity from the angular momentum conservation law as follows[1,5]:

$$\dot{\epsilon} = \boldsymbol{H}\dot{\boldsymbol{q}} \tag{1}$$

On the other hand, the relationship between the end-effector velocity and the joint angle velocity satisfies the following equation[1,8]:

$$\dot{\boldsymbol{u}} = \boldsymbol{J}\dot{\boldsymbol{q}} \tag{2}$$

When the number of the manipulator joints is six, $\boldsymbol{u}$ and $\boldsymbol{q}$ are diffeomorphic except for the singular points. Because we use the Euler parameters as the orientation elements, $\boldsymbol{u}$ has seven coordinates and $\boldsymbol{J}$ is a 7 × 6 matrix. We represent the orientation by four coordinates. However, the minimum required dimensions are three, and the orientation space is non-Euclidean and has several singular points with only three coordinates. We adopt the Euler parameters because they represent the orientation by four coordinates with a constraint that its norm equals 1 and there has no singular point in its space. Consequently, our coordinates are expressed by more coordinates than required. When the Jacobian $\boldsymbol{J}$ is full rank, the solution $\dot{\boldsymbol{q}}$ for a physically consistent $\dot{\boldsymbol{u}}$ is obtained as follows:

$$\dot{\boldsymbol{q}} = \boldsymbol{J}^{\sharp}\dot{\boldsymbol{u}} \tag{3}$$

Adopting the differential form,[9,10] the equation of motion of the whole system is obtained from Eqs. (1) and (3) as follows:

$$d\boldsymbol{x} = \boldsymbol{X}\,d\boldsymbol{u} \tag{4}$$

III. Planning the Spiral Motion

In Sec. III.A, we yield an approximate closed trajectory for a single-turn spiral motion connecting the start and endpoints of the desired trajectory. Then, we describe in Sec. III.B a method finding a locally optimal solution about the approximate solution obtained in Sec. III.A. In Sec. III.C, we describe a method for searching the exact solution of the spiral motion. Finally, we state a method for computing a multiturn spiral motion in Sec. III.D to obtain the solution for the arbitrary given nonzero allowance of approximation.

Yamada[5] proposed a variational method to find an optimal solution taking joint coordinates as the space for trajectory planning. We take the $\boldsymbol{R}^3 \times \boldsymbol{S}^3$ space of end-effector position and orientation as the space for trajectory planning and express it with seven variables using Euler parameters. As the computational algorithm of optimization, we adopt Yamada's method.

A. Single-Turn Spiral Motion

We derive the formula of closed trajectory motion that results in an arbitrary change of satellite orientation by using the differential form and Lie bracket. The desired trajectory $\boldsymbol{x}_d$ is generally infeasible. We express the nominal motion of the end effector along the desired trajectory as $\boldsymbol{u}_n(t) \overset{\text{def}}{=} \boldsymbol{u}_d(t)$. The difference between $\boldsymbol{u}$ and $\boldsymbol{u}_n$ is expressed as $\boldsymbol{u}_c(t) \overset{\text{def}}{=} \boldsymbol{u}(t) - \boldsymbol{u}_n(t)$. When $\boldsymbol{u}$ connects the start and endpoints of the desired trajectory, $\boldsymbol{u}_c$ becomes a closed path.

A feasible trajectory of $\boldsymbol{x}$ connecting the start and endpoints of the desired trajectory is obtained from Eq. (4):

$$\Delta\boldsymbol{x}(t) = \boldsymbol{x}_0 + \int_{t_0}^{t} \boldsymbol{X}\dot{\boldsymbol{u}}\,dt \tag{5}$$

The change of generalized coordinates by $\boldsymbol{u}_n$ becomes as follows:

$$\Delta\boldsymbol{x}_n(t) = \boldsymbol{x}_0 + \int_{t_0}^{t} \boldsymbol{X}_n\dot{\boldsymbol{u}}_n\,dt \tag{6}$$

Let

$$\begin{aligned} \boldsymbol{x}_c(t) &\overset{\text{def}}{=} \boldsymbol{x}(t) - \boldsymbol{x}_n(t) \\ &= \int_{t_0}^{t} (\boldsymbol{X}\dot{\boldsymbol{u}} - \boldsymbol{X}_n\dot{\boldsymbol{u}}_n)\,dt \end{aligned} \tag{7}$$

Adopting the differential form, Eq. (7) becomes

$$d\boldsymbol{x}_c = \boldsymbol{X}\,d\boldsymbol{u} - \boldsymbol{X}_n\,d\boldsymbol{u}_n \tag{8}$$

Differentiating Eq. (8), from Eq. (4) we obtain

$$d(d\boldsymbol{x}_c) = \frac{\partial\boldsymbol{X}}{\partial\boldsymbol{x}}\boldsymbol{X}\,d\boldsymbol{u}_c \wedge d\boldsymbol{u}_c + \left(\frac{\partial\boldsymbol{X}}{\partial\boldsymbol{x}}\boldsymbol{X} - \frac{\partial\boldsymbol{X}_n}{\partial\boldsymbol{x}}\boldsymbol{X}_n\right) d\boldsymbol{u}_n \wedge d\boldsymbol{u}_n \tag{9}$$

The first term of Eq. (9) implies the change of generalized coordinates due to the closed trajectory motion. The second term indicates the effect due to the $\boldsymbol{u}_n$. In the case that the desired trajectory is sufficiently short, $\boldsymbol{u}_n$ can be considered small. On the other hand, in the case that the spiral trajectory is sufficiently near to the desired trajectory, ϵ nearly equals ϵ_n. In both cases, the second term in Eq. (9) can be neglected. In this section and the next, we consider only the first term and neglect the second one. Now, $d(d\epsilon_c)$ becomes the function of only $\boldsymbol{u}_c$. $\Delta\epsilon_c$ is obtained from Stokes theorem,[5,9] and Eq. (9) becomes as follows:

$$\begin{aligned} \Delta\boldsymbol{x}_c = \int_C d\boldsymbol{x}_c &= \int_S d\,(d\boldsymbol{x}_c) \\ &= \int_S \sum_{i,j} \frac{\partial\boldsymbol{X}_j}{\partial\boldsymbol{x}}\boldsymbol{X}_i\,du_{c,i} \wedge du_{c,j} \end{aligned} \tag{10}$$

We express the closed trajectory $\boldsymbol{u}_c$ using two parameters s_1 and s_2 as

$$\boldsymbol{u}_c = \boldsymbol{a}s_1 + \boldsymbol{b}s_2 + \boldsymbol{c} \tag{11}$$

For simplicity and smoothness of the spiral trajectory, we propose to express s_1 and s_2 by sinusoidal functions as

$$s_1 = \cos\phi(t - t_0) \qquad s_2 = \sin\phi(t - t_0) \tag{12}$$

The closed trajectory $\boldsymbol{u}_c$ becomes elliptical. The $\boldsymbol{a}$ and $\boldsymbol{b}$ denote two radii of the ellipse. From Eq. (A2), $\epsilon^T\epsilon = 1$ always must be satisfied. Considering the case where $s_1 = 1$ and $s_2 = 0$ and other cases, Eqs. (11) and (12) yield the following constraints for the orientational elements (lower four components) of $\boldsymbol{a}$, $\boldsymbol{b}$, and $\boldsymbol{c}$:

$$\boldsymbol{a}_\epsilon^T\boldsymbol{b}_\epsilon = \boldsymbol{a}_\epsilon^T\boldsymbol{c}_\epsilon = \boldsymbol{b}_\epsilon^T\boldsymbol{c}_\epsilon = 0 \qquad \boldsymbol{a}_\epsilon^T\boldsymbol{a}_\epsilon = \boldsymbol{b}_\epsilon^T\boldsymbol{b}_\epsilon = 1 - \boldsymbol{c}_\epsilon^T\boldsymbol{c}_\epsilon \tag{13}$$

These are the additional constraints to be satisfied when we carry out our optimization in $\boldsymbol{R}^3 \times \boldsymbol{S}^3$ rather than in $\boldsymbol{R}^6$.

Adopting Eq. (11), Eq. (10) can be alternatively represented by Lie bracket[9,10]:

$$\begin{aligned} \Delta\boldsymbol{x}_c &= \int_E \sum_{i,j} \left(a_i b_j \frac{\partial\boldsymbol{X}_j}{\partial\boldsymbol{x}}\boldsymbol{X}_i - a_j b_i \frac{\partial\boldsymbol{X}_j}{\partial\boldsymbol{x}}\boldsymbol{X}_i \right) dE \\ &= \sum_{i,j} a_i b_j \int_E [\boldsymbol{X}_i, \boldsymbol{X}_j]\,dE \\ &= \boldsymbol{a}^T\boldsymbol{D}\boldsymbol{b} \end{aligned} \tag{14}$$

where $\boldsymbol{D}$ denotes a 7×7 tensor whose (i, j) element is defined as

$$\boldsymbol{D}_{ij} \overset{\text{def}}{=} \int_E [\boldsymbol{X}_i, \boldsymbol{X}_j]\,dE \tag{15}$$

Note that the satellite orientation change is expressed in terms of Lie brackets of column vectors of $\boldsymbol{X}$ and, because the lower part of $\boldsymbol{x}$ is the input $\boldsymbol{u}$ itself, the lower parts of $\boldsymbol{x}_c$ and $\boldsymbol{D}_{ij}$ are equivalently zero. It is a rather simpler formulation of the effect than that of Yamada's.

B. Computation of Single-Turn Spiral Motion

There are many solutions of the closed trajectory $\boldsymbol{u}_c$. We choose one that minimizes a certain criterion in this section. The $\boldsymbol{u}_c$ has three unknown vectors, $\boldsymbol{a}$, $\boldsymbol{b}$, and $\boldsymbol{c}$, as seen in Eq. (11). Because $\boldsymbol{c}$ is determined from $\boldsymbol{a}$, $\boldsymbol{b}$, and the initial conditions, our goal in this section is to find minimal $\boldsymbol{a}$ and $\boldsymbol{b}$.

Specifically, we use $Q = \boldsymbol{a}^T\boldsymbol{W}\boldsymbol{a} + \boldsymbol{b}^T\boldsymbol{W}\boldsymbol{b}$ as the criterion to minimize. The criterion can be equivalently represented by

$$Q = (1/\phi^2)\left((1/L^2)\boldsymbol{v}_e^T\boldsymbol{v}_e + \tfrac{1}{4}\boldsymbol{\omega}_e^T\boldsymbol{\omega}_e\right) \tag{16}$$

when we used the relation of Eq. (A3). Namely, our criterion is interpreted as minimizing a normalized end-effector velocity.

In what follows, we carry out optimization as if our problem would lie in $\boldsymbol{R}^7$ rather than $\boldsymbol{R}^3 \times \boldsymbol{S}^3$. Namely, we disregard the constraints of Eq. (13) between the lower four components of $\boldsymbol{u}$. This allows us to use Yamada's algorithm as it is. We summarize it in Appendix B for the readers' convenience. At the end of this subsection, we show that the optimal solution thus obtained automatically satisfies the constraints of Eq. (13).

$\boldsymbol{D}$ in Eq. (14) is a fairly complex function of $\boldsymbol{a}$ and $\boldsymbol{b}$. Yamada's algorithm assumes that the integrands of Eqs. (6) and (15) are constant and invariant to $\boldsymbol{a}$ and $\boldsymbol{b}$. The error due to this assumption will be corrected in the next section when we compute the exact solution. Therefore, $\boldsymbol{x}(t_0 + \Delta t)$ can be represented from Eqs. (6), (7), and (14) as

$$\boldsymbol{x}(t_0 + \Delta t) = \boldsymbol{x}(t_0) + \Delta \boldsymbol{x}_n + \boldsymbol{a}^T \boldsymbol{D} \boldsymbol{b} \tag{17}$$

where $\Delta \boldsymbol{x}_n$ can be calculated as

$$\Delta \boldsymbol{x}_n = \boldsymbol{X}(\boldsymbol{u}_n(t_0 + \Delta t) - \boldsymbol{u}_n(t_0)) \tag{18}$$

and Eq. (15) is rewritten as

$$\boldsymbol{D}_{ij} = \left\{ \begin{matrix} \left(\dfrac{\partial \boldsymbol{Y}_j}{\partial u_i} - \dfrac{\partial \boldsymbol{Y}_i}{\partial u_j} + \dfrac{\partial \boldsymbol{Y}_j}{\partial \epsilon} \boldsymbol{Y}_i - \dfrac{\partial \boldsymbol{Y}_i}{\partial \epsilon} \boldsymbol{Y}_j \right) E \\ \boldsymbol{0} \end{matrix} \right\} \tag{19}$$

The partial derivatives in Eq. (19) are obtained by numerical differentiation. This needs some consideration because ϵ are the Euler parameters and are constrained on a unit four-dimensional hypersphere. We propose a method of numerical differentiation with Euler parameters in the second subsection of Appendix A.

To summarize the procedure, we calculate a single-turn spiral motion as follows:

1) Let $\boldsymbol{u}_n = \boldsymbol{u}_d(t)$, and then calculate $\Delta \epsilon_n$.

2) Solve a closed trajectory motion $\boldsymbol{u}_c$ (or, equivalently, $\boldsymbol{a}$ and $\boldsymbol{b}$), which satisfies $\Delta \epsilon_c = \Delta \epsilon_d - \Delta \epsilon_n$ according to Yamada's algorithm in Appendix B.

3) Letting $\boldsymbol{u} = \boldsymbol{u}_n + \boldsymbol{u}_c$, compute a single-turn spiral motion trajectory connecting the start and endpoints of the desired trajectory.

From Eq. (B7), the optimal solutions of $\boldsymbol{a}$ and $\boldsymbol{b}$ just obtained satisfy

$$\boldsymbol{a}^T \boldsymbol{W} \boldsymbol{b} = 0 \qquad \boldsymbol{a}^T \boldsymbol{W} \boldsymbol{a} = \boldsymbol{b}^T \boldsymbol{W} \boldsymbol{b} = -\tfrac{1}{2} \boldsymbol{\lambda}^T \Delta \epsilon_{cd} \tag{20}$$

For any choices of L in $\boldsymbol{W}$, the optimal solution thus obtained automatically satisfies the constraints of Eq. (13).

C. Searching for an Exact Solution

The preceding solution is no more than an approximate solution because $\Delta \epsilon_n$ and $\boldsymbol{D}$ are calculated only by initial condition and the effect of $\boldsymbol{u}_n$ for ϵ_c is not considered. Searching for the exact solution, we first calculate the motion of the space robot using the approximate solution and calculate $\Delta \epsilon$. Then we search for an exact solution by iterative calculation with Newton's method,

$$\begin{pmatrix} \boldsymbol{a}^{(i)} \\ \boldsymbol{b}^{(i)} \end{pmatrix} = \begin{pmatrix} \boldsymbol{a}^{(i-1)} \\ \boldsymbol{b}^{(i-1)} \end{pmatrix} - \begin{pmatrix} \dfrac{\partial \Delta \epsilon}{\partial \boldsymbol{a}} & \dfrac{\partial \Delta \epsilon}{\partial \boldsymbol{b}} \end{pmatrix}^{\sharp} (\Delta \epsilon - \Delta \epsilon_d) \tag{21}$$

where the second term of the right-hand side is calculated using $\boldsymbol{a}^{(i-1)}, \boldsymbol{b}^{(i-1)}$.

Note that though the approximate solution requires only the initial and final values of $\boldsymbol{u}_n$, $\Delta \epsilon$ is calculated while searching for the exact solution by the following integration:

$$\Delta \epsilon = \int_{t_0}^{tf} \boldsymbol{Y}(\dot{\boldsymbol{u}}_n + \dot{\boldsymbol{u}}_c)\, dt \tag{22}$$

Therefore, the exact solution follows the desired trajectory.

D. Multiturn Spiral Motion

Previously, we proposed the single-turn spiral motion, which connects the start and end-points of an arbitrary nine-dimensional trajectory. However, if the environment of a space robot is surrounded by obstacles, the space robot should avoid them. In this subsection, we propose the multiturn spiral motion, which enables one to approximately follow an arbitrary nine-dimensional trajectory with an arbitrary margin.

From Eq. (20), σ implies the radius of closed trajectory. The spiral frequency of single-turn spiral motion from $t = t_0$ to $t = t_0 + \Delta t$ is $\phi_1 = 2\pi/\Delta t$ and E in Eq. (19) becomes $E = \phi_1 \Delta t / 2 = \pi$. For multiturn spiral motion within Δt, the spiral frequency is represented by $\phi_n = n\phi_1 = 2n\pi/\Delta t$ and, therefore, $E = \phi_n \Delta t/2 = n\pi$. Because E is proportional to spiral pitch n, $\boldsymbol{D}$ is proportional to n from Eq. (19), and σ^2 is inversely proportional to n from Eq. (14). Accordingly, it is inversely proportional to ϕ. Namely,

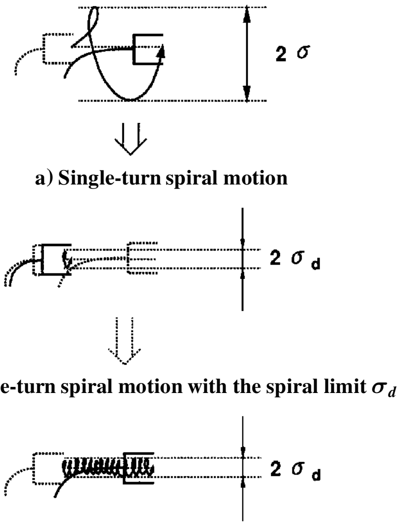

a) Single-turn spiral motion

b) Single-turn spiral motion with the spiral limit σ_d

c) Multiturn sprial motion with the spiral limit σ_d

Fig. 1 Multiturn spiral motion planning.

$$\sigma^2 \propto (1/n) \propto (1/\phi) \tag{23}$$

Therefore, the larger the spiral pitch (that is, faster the spiral frequency) is, the smaller the spiral radius is.

We describe a method to solve a multiturn spiral motion by imposing σ_d.

1) Set $n^{(0)} = 1$.

2) Calculate $\Delta t = (t_f - t_0)/n$ and $\phi = 2\pi/\Delta t$.

3) Solve a single-turn spiral motion with ϕ in step 2. Obtain the spiral radius σ.

4) Compute $n^{(k)}$ by rounding up $n^{(k-1)} \times (\sigma/\sigma_d)^2$ to the nearest whole number.

5) If $n^{(k)} = n^{(k-1)}$, then the $n^{(k)}$ gives the maximum single-turn spiral motion, with the spiral limit σ_d. Otherwise, return step 2.

6) Compute the next spiral starting from the end of the previous spiral. Set $n^{(0)} = n^{(k)} - 1$. Go to step 2.

A multiturn spiral trajectory approximating the desired trajectory within the spiral limit can be solved by this procedure. We illustrate the procedure in Fig. 1.

Because the spiral perturbation is determined repeatedly, at each cycle, it can be designed to reduce the motion error generated or accumulated in the previous cycles. This implies the method, if computed in real time with faster computers in the future, is suitable as a feedback control method.

IV. Computer Simulation

The lengths, mass, and inertia matrices of the satellite and each link of the space robot are assumed as given in Table 1, where the 0th link denotes the base satellite. The arrangement of each link and joint is given in Fig. 2. The satellite [link(0)] is a cylinder, the radius of which is 2 m, represented as $\phi 2$ in Fig. 2 and Table 1, and the height is 1 m. The positions of the center of gravity of each link are assumed at the geometric center of the link.

The initial state of the space robot is $\boldsymbol{q} = (\pi/3, -\pi/3, \pi/3, -\pi/3, \pi/3, -\pi/3)^T$ rad with the configuration of Fig. 2 as the origin. The desired trajectory of the end effector is to move it for 1s at the constant speed 0.5 m/s in the positive x-axis direction and to maintain its orientation. That of the satellite orientation is to maintain the satellite orientation. The initial configuration and the desired trajectory are given in Fig. 3, where the broken line stretched from the end effector denotes the desired trajectory.

Figure 4 shows the satellite orientation variation in response to the end-effector desired trajectory without spiral motion. The solid, broken, and chain lines denote the three vector elements of Euler parameters, e_1, e_2, and e_3, respectively. Figure 5 shows the same motion every 0.2 s.

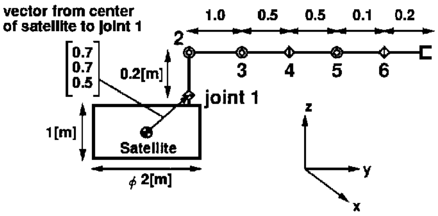

Fig. 2 Structure of a space robot: q_i denotes the angle of the joint i, rad.

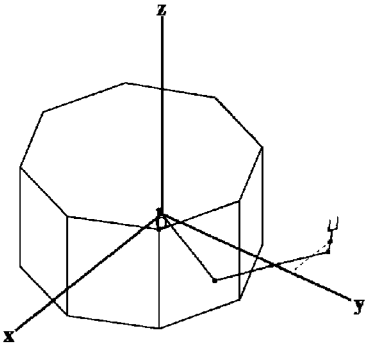

Fig. 3 Initial configuration of the space robot.

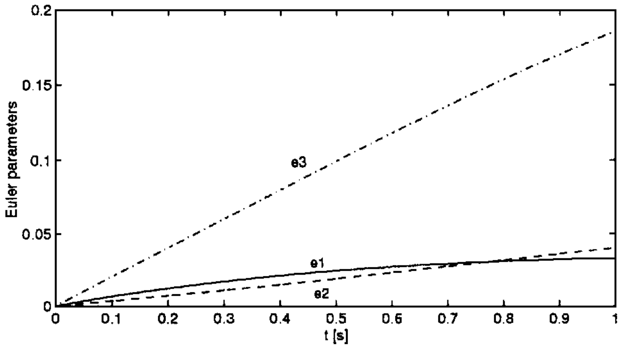

Fig. 4 Satellite orientation variation: Δu_x = 0.5 m, without spiral motion.

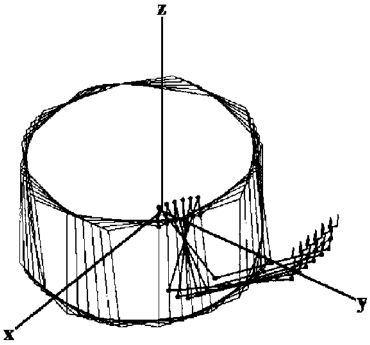

Fig. 5 Movements of the space robot: Δu_x = 0.5 m, without spiral motion.

Table 1 Link parameters

Link	Length, m	Mass, kg	Inertia, kg · m^2		
0	$\phi 2 \times 1$	500	100	100	100
1	0.2	10	0.1	0.1	0.1
2	1.0	30	3	0.2	3
3	0.5	20	0.5	0.2	0.5
4	0.5	20	0.5	0.2	0.5
5	0.1	10	0.1	0.1	0.1
6	0.2	20	0.1	0.1	0.1

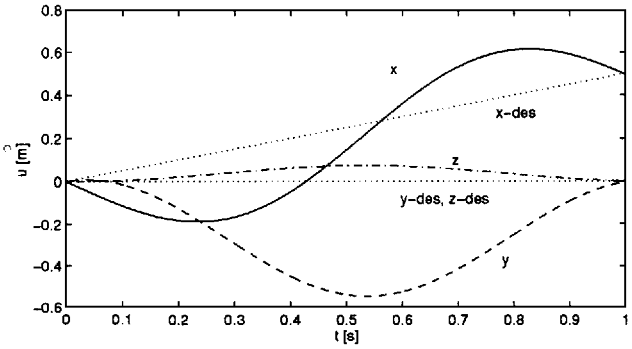

Fig. 6 End-effector coordinates variation: Δu_x = 0.5 m, single-turn spiral motion.

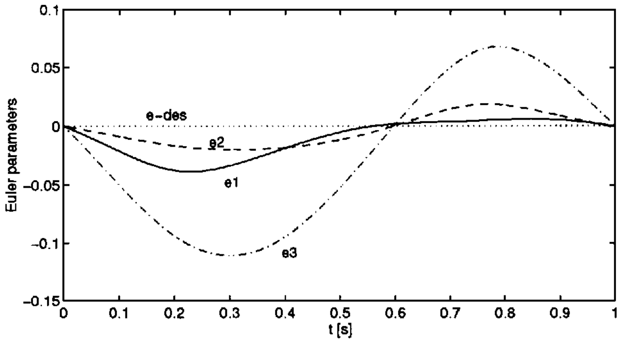

Fig. 7 Satellite orientation variation: Δu_x = 0.5 m, single-turn spiral motion.

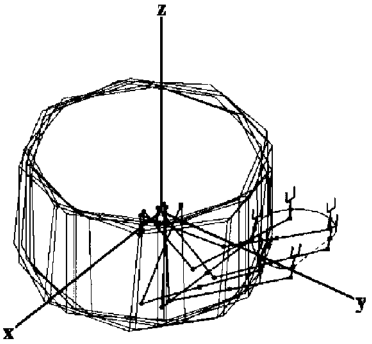

Fig. 8 Movements of the space robot: Δu_x = 0.5 m, single-turn spiral motion.

The results of single-turn spiral motion are shown in Figs. 6–8. In Fig. 6, the solid line denotes the end-effector coordinate x variation, the broken and the chain lines denote y and z. The dotted lines denote each desired trajectories. Figure 7 shows the satellite orientation variation. Figure 8 illustrates the motion every 0.2 s.

Figures 9–11 correspond to the multiturn spiral motion when the spiral radius limit σ_d sets at 0.1 m. Figures 9 and 10, similar to Figs. 6 and 7, show the end-effector coordinate variation and the satellite orientation variation. Figure 11 illustrates the motion, where we plotted only the trajectory of the end-effector position. The satellite with the solid line denotes the final state and that with the broken line denotes the initial state. Note that the satellite makes a small fluctuation in Fig. 10 while making a multiturn spiral motion.

From Figs. 4 and 5, it is seen that the satellite orientation would be subject to a great disturbance when following the end-effector desired trajectory. When spiral motion is applied, a trajectory connecting the start and endpoints is obtained as shown in Figs. 6–11. Especially, in Figs. 9–11, the infeasible desired trajectory is approximated with the desired spiral radius. If the spiral limit σ_d is chosen smaller, one can get a multiturn spiral motion with a better approximation. Because ϕ is inversely proportional to σ_d^2, the motion becomes much faster in this case.

Similar simulations are done for all three axes of x, y, and z and show almost similar results. The computational time by Sun SPARC station 10 is shown in Table 2 for each case of none, single-turn, and multiturn spiral motion.

V. Effects of Singularity

In the course of the computer simulation, we found that for some desired trajectories there are cases where the searching convergence

Table 2 Computational time

Computational time, s		Spiral motion		
		None	Single	Multi
Direction	x	20	3.0×10^3	5.7×10^3
	y	20	3.7×10^3	——
	z	20	3.0×10^3	3.5×10^3

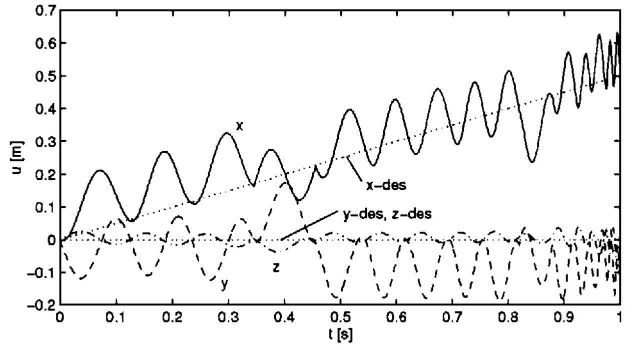

Fig. 9 End-effector coordinates variation: Δu_x = 0.5 m, multiturn spiral motion.

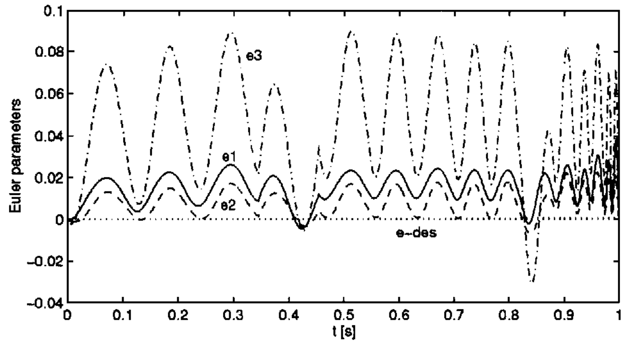

Fig. 10 Satellite orientation variation: Δu_x = 0.5 m, multiturn spiral motion.

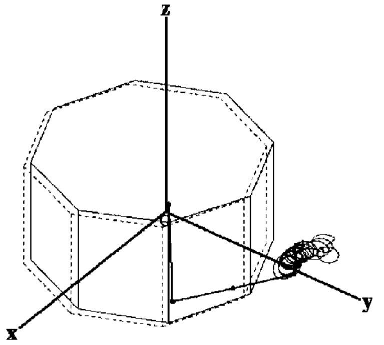

Fig. 11 Movements of the space robot: Δu_x = 0.5 m, multiturn spiral motion.

to the exact solution becomes very slow. This happens when the system passes by the neighborhood of a singular point in the trajectory. We investigated the relationship between singularity and convergence of the solution with spiral radius in the cases of multiturn spiral motions in Figs. 9–11. The results are shown in Fig. 12. Figure 12a shows magnitudes of the spiral radius, normalized by the spiral period $\Delta t = (t_f - t_0)/n$, where the solid line and empty circles denote $\|\boldsymbol{a}\|_W/\sqrt{(\Delta t)}$. The broken line and crosses denote $\|\boldsymbol{b}\|_W/\sqrt{(\Delta t)}$. Figure 12b shows the number of iterations in each period of single-turn spiral motion, normalized by the spiral period Δt. Figure 12c shows variations of the condition numbers, where the solid line and empty circles denote the condition numbers of $\boldsymbol{Y}$ in the motion, and the broken line and crosses denote the condition number of the generalized Jacobian $\boldsymbol{J}$.

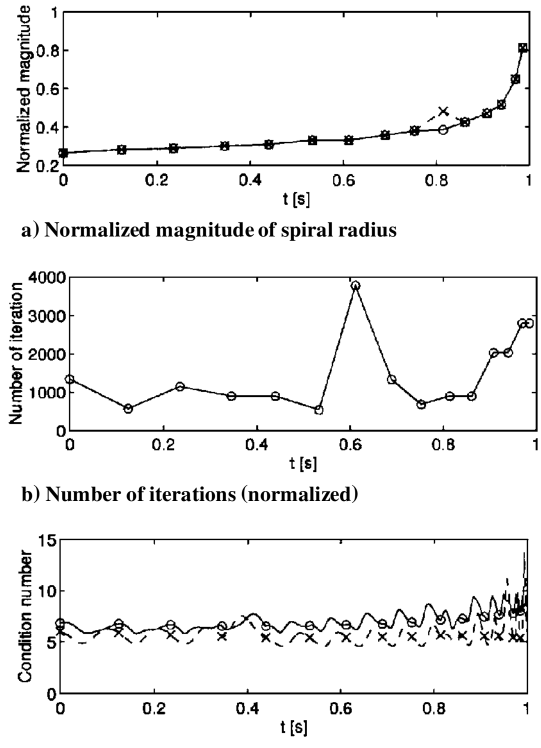

a) Normalized magnitude of spiral radius

b) Number of iterations (normalized)

c) Condition number

Fig. 12 Effects of singular points: Δu_x = 0.5 m, multiturn spiral motion.

From Fig. 12, we can see that after the condition number becomes larger near $t = 0.7$ and 0.9 s, the spiral radius and the number of iterations become larger suddenly near $t = 0.8$ and 1.0 s. Iterative calculation should continue until the error becomes sufficiently small. In practice, however, when the number of iterations became too large we terminated the iteration and advanced to the next spiral. Although some error remained, we expect the error to be resolved in the subsequent step. The convergence that actually resulted was worse, because a larger orientation error had to be resolved in the following steps. This seems to be reason that the number of iterations tends to be large at the end of motion after the neighborhood of singular points. The singularities would also reduce the accuracy of the calculation particularly for small spiral radii. The resolution of this problem belongs to the open problem. In a practical sense, the spiral radii should be maximized within the designated margin.

VI. Conclusion

Space robots cannot realize arbitrary motion of the manipulator and the satellite only by actuation of manipulator joints.

1) We proposed a method to approximate infeasible motions by spiral-like perturbations around the desired trajectory of the end effector, with an arbitrary nonzero maximum allowance.

2) We formulated a change of satellite orientation with end-effector trajectory in the non-Euclidean space $\boldsymbol{R}^3 \times S^3$. We extended a variational method for optimization and obtained the optimal spiral motion.

3) We proposed a multiturn spiral motion and constituted a method to solve it by imposing the upper limit of the spiral radius.

4) We showed the effectiveness of computation by computer simulation. In the course of the simulation, we pointed out the problem that convergence becomes slow after passing through neighborhoods of singular points. It would be one of the open problems.

Appendix A: Euler Parameters

Definition and Properties

The Euler parameters are defined as a quaternion and are represented by a point on the surface of four-dimensional unit hypersphere S^3. The Euler parameters ϵ, namely, orientations from the standard orientation, are expressed by the rotation axis $\boldsymbol{n}$ and the rotation angle θ about the axis as follows[11,12]:

$$\epsilon = \begin{Bmatrix} \cos(\theta/2) \\ \sin(\theta/2)\boldsymbol{n} \end{Bmatrix} = \begin{Bmatrix} e_0 \\ e_1 \\ e_2 \\ e_3 \end{Bmatrix} \in \boldsymbol{S}^3 \tag{A1}$$

Note that the orientation space is a non-Euclidean space, $\boldsymbol{S}^3$. Namely, the Euler parameters have the following constraints:

$$\boldsymbol{\epsilon}^T \boldsymbol{\epsilon} = 1 \tag{A2}$$

The relation between Euler parameters and angular velocity is expressed as

$$\boldsymbol{\omega} = 2\dot{\boldsymbol{\epsilon}}\boldsymbol{\epsilon}^* \tag{A3}$$

Numerical Differentiation with Euler Parameters

We perform numerical differentiation using the Gibbs vector and its transformation $\partial/\partial\epsilon = (d\boldsymbol{\xi}/d\epsilon)(\partial/\partial\boldsymbol{\xi})$. The relationship between the Gibbs vector and the Euler parameters is as follows. For

$$\epsilon = \begin{Bmatrix} e_0 \\ e_1 \\ e_2 \\ e_3 \end{Bmatrix}$$

$\boldsymbol{\xi}$ is given as

$$\boldsymbol{\xi} = \frac{1}{e_0}\begin{pmatrix} e_1 \\ e_2 \\ e_3 \end{pmatrix}$$

Then

$$\frac{\partial \boldsymbol{\xi}}{\partial \epsilon} = \frac{1}{e_0^2}\begin{pmatrix} -e_1 & e_0 & 0 & 0 \\ -e_2 & 0 & e_0 & 0 \\ -e_3 & 0 & 0 & e_0 \end{pmatrix} \tag{A4}$$

Appendix B: Yamada's Algorithm of Optimization

Yamada[5] considered the change of satellite orientation when the manipulator makes a closed trajectory motion in joint space. When the manipulator joints follow a closed trajectory of $\boldsymbol{q} = \boldsymbol{a}_q s_1 + \boldsymbol{b}_q s_2 + \boldsymbol{c}_q$, where parameters s_1 and s_2 make a closed path in their space, the satellite orientation change $\Delta\epsilon$ is obtained as

$$\Delta\epsilon = \boldsymbol{a}_q^T \boldsymbol{D}_q \boldsymbol{b}_q \tag{B1}$$

where $\boldsymbol{D}_q$ denotes a 6×6 tensor whose (i, j) element is defined as

$$\boldsymbol{D}_{q,ij} = \int_E \left(\frac{\partial \boldsymbol{f}_i}{\partial \boldsymbol{q}_j} - \frac{\partial \boldsymbol{f}_j}{\partial \boldsymbol{q}_i} + \boldsymbol{f}_i \times \boldsymbol{f}_j \right) \epsilon \, dE \tag{B2}$$

where $\boldsymbol{f}_i$ is defined by the equation between the satellite angular velocity and joint velocity as

$$\boldsymbol{\omega} = -\sum_{i=1}^{n} \boldsymbol{f}_i \dot{q}_i \tag{B3}$$

Let the criterion Q be

$$Q = \boldsymbol{a}_q^T \boldsymbol{a}_q + \boldsymbol{b}_q^T \boldsymbol{b}_q \tag{B4}$$

Adding this criterion Q and the constraint $\epsilon = \epsilon_d$ and using Lagrange multiplier $\boldsymbol{\lambda}$, the augmented criterion J is represented by

$$J = \boldsymbol{a}_q^T \boldsymbol{a}_q + \boldsymbol{b}_q^T \boldsymbol{b}_q + \boldsymbol{\lambda}^T (\Delta\epsilon - \Delta\epsilon_d) \tag{B5}$$

which is to be minimized with the variational method.

The necessary condition of the optimal solution is that J has a stationary value at $\boldsymbol{a}_q$ and $\boldsymbol{b}_q$. Then, it is expressed as

$$\left(\frac{\partial J}{\partial \boldsymbol{a}_q}\right)^T = 2\boldsymbol{a}_q + \left(\frac{\partial \Delta\epsilon}{\partial \boldsymbol{a}_q}\right)^T \boldsymbol{\lambda} = \boldsymbol{0}$$
$$\left(\frac{\partial J}{\partial \boldsymbol{b}_q}\right)^T = 2\boldsymbol{b}_q + \left(\frac{\partial \Delta\epsilon}{\partial \boldsymbol{b}_q}\right)^T \boldsymbol{\lambda} = \boldsymbol{0} \qquad \Delta\epsilon - \Delta\boldsymbol{\epsilon}_{\mathbf{d}} = \boldsymbol{0} \tag{B6}$$

On the basis of the assumption that the integrand of Eq. (B2) is constant and invariant to $\boldsymbol{a}_q$ and $\boldsymbol{b}_q$, Eq. (B6) can be rewritten as

$$2\boldsymbol{a}_q + \boldsymbol{D}_{q\lambda}\boldsymbol{b}_q = \boldsymbol{0} \qquad 2\boldsymbol{b}_q - \boldsymbol{D}_{q\lambda}\boldsymbol{a}_q = \boldsymbol{0} \tag{B7}$$

where $\boldsymbol{D}_{q\lambda}$ denotes a 6×6 matrix whose (i, j) element is

$$D_{q\lambda,ij} \overset{\text{def}}{=} \sum_k D_{q,ijk}\lambda_k \tag{B8}$$

and $\boldsymbol{D}_{q\lambda}$ is skew symmetric from Eq. (B2).

From Eq. (B7), we have $\boldsymbol{b}_q = \frac{1}{2}\boldsymbol{D}_{q\lambda}\boldsymbol{a}_q$, and Eq. (B6) yields the nonlinear simultaneous equations as

$$\boldsymbol{D}_{qa}^T \boldsymbol{D}_{qa} \boldsymbol{\lambda} + 2\Delta\epsilon_d = \boldsymbol{0} \tag{B9}$$

$$\left(\boldsymbol{I} + \tfrac{1}{4}\boldsymbol{D}_{q\lambda}^2\right)\boldsymbol{a}_q = \boldsymbol{0} \tag{B10}$$

where $\boldsymbol{D}_{qa}$ denotes a 6×4 matrix whose (i, k) element is

$$D_{qa,ik} \overset{\text{def}}{=} \sum_j D_{q,ijk} a_{q,j} \tag{B11}$$

Solving Eqs. (B9) and (B10), we find solutions $\boldsymbol{a}_q$, $\boldsymbol{b}_q$, and $\boldsymbol{\lambda}$ satisfying Eq. (B6).

Acknowledgment

This research was in part supported by the Toyota Physical and Chemical Research Institute and Grant in Aid of Scientific Research from the Ministry of Culture and Education, General Research (B)04452153. Discussions with Ken'ichi Yoshimoto of the Department of Mechano-Informatics, University of Tokyo, were essential for accomplishing this work.

References

[1] Nakamura, Y., and Mukherjee, R., "Nonholonomic Path Planning of Space Robots via a Bidirectional Approach," *IEEE Transactions on Robotics and Automation,* Vol. 7, No. 4, 1991, pp. 500–514.

[2] Vafa, Z., and Dubowsky, S., "On the Dynamics of Space Manipulators Using the Virtual Manipulator, with Applications to Path Planning," *Journal of the Astronautical Sciences,* Vol. 38, No. 4, 1990, pp. 441–472.

[3] Senda, K., Murotsu, Y., and Ozaki, M., "A Method of Attitude Control for Space Robots (An Approach Using a Neural Network)," *Transactions of the Japan Society of Mechanical Engineers,* Vol. 57, No. 539 (C), 1991, pp. 2356–2362.

[4] Akiyama, T., and Sakawa, Y., "Path Planning of Space Robots by Nonlinear Programming," *Robotic Society of Japan 3rd Robot Symposium,* 1993, pp. 191–196.

[5] Yamada, K., "Arm Path Planning for a Space Robot," *Proceedings of the 1993 Institute of Electrical and Electronics Engineers/Robotic Society of Japan International Conference on Intelligent Robots and Systems*, 1993, pp. 2049–2055.

[6] Brockett, R.-W., "Asymptotic Stability and Feedback Stabilization," *Differential Geometric Control Theory*, edited by R. Brockett, R. Millman, and H. Sussman, Vol. 27, Progress in Mathematics, 1983, pp. 181–208.

[7] Sampei, M., Ishikawa, M., Kiyota, H., and Koga, M., "Time-State Control Form and Its Application to Non-Holonomic Systems," *12th Annual Conference of the Robotic Society of Japan,* No. 2, 1994, pp. 437–438.

[8] Umetani, Y., and Yoshida, K., "Continuous Path Control of Space Manipulators Mounted on OMV," *Acta Astronautica,* Vol. 15, No. 12, 1987, pp. 981–986.

[9] Schutz, B.-F., *Geometrical Method of Mathematical Physics*, Cambridge Univ. Press, London, 1980, Chap. 2.

[10] Varadarajan, V.-S., *Lie Groups, Lie Algebras, and Their Representations*, edited by P.-R. Halmos, F.-W. Gehring, and C.-C. Moore, No. 102, Graduate Texts in Mathematics, Springer–Verlag, New York, 1984, pp. 46–51.

[11] Spring, K.-W., "Euler Parameters and the Use of Quaternion Algebla in the Manipulation of Finite Rotations, a Review," *Mechanism and Machine Theory,* Vol. 21, No. 5, 1986, pp. 365–373.

[12] Chou, J.-C.-K., "Quaternion Kinematic and Dynamic Differential Equations," *IEEE Transactions on Robotics and Automation,* Vol. 8, No. 1, 1992, pp. 53–64.

F. H. Lutze Jr.
Associate Editor